The Evolution of Dust Opacity in Core Collapse Supernovae and the Rapid Formation of Dust in Their Ejecta

Eli Dwek[1], Arkaprabha Sarangi[1], and Richard G. Arendt[2]
Observational Cosmology Lab, NASA Goddard Space Flight Center, Mail Code 665, Greenbelt, MD 20771, USA; eli.dwek@nasa.gov

Abstract

Infrared (IR) observations of core collapse supernovae (CCSNe) have been used to infer the mass of dust that has formed in their ejecta. A plot of inferred dust masses versus supernova (SN) ages shows a trend of increasing dust mass with time, spanning a few decades of observations. This trend has been interpreted as evidence for the slow and gradual formation of dust in CCSNe. Observationally, the trend exhibits a t^2 behavior, exactly what is expected from an expanding optically thick ejecta. In this case, the observed dust resides in the IR-thin "photosphere" of the ejecta, and constitutes only a fraction of the total dust mass. We therefore propose that dust formation proceeds very rapidly, condensing most available refractory elements within two years after the explosion. At early epochs, only a fraction of the dust emission escapes the ejecta accounting for the low observed dust mass. The ejecta's entire dust content is unveiled only a few decades after the explosion, with the gradual decrease in its IR opacity. Corroborating evidence for this picture includes the early depletions of refractory elements in the ejecta of SN1987A and the appearance of a silicate emission band around day 300 in SN 2004et.

Key words: astrochemistry – dust, extinction – molecular processes – nuclear reactions, nucleosynthesis, abundances – supernovae: general

1. Introduction

Core collapse supernovae (CCSNe) drive the chemical enrichment of galaxies and are potentially the most important source of interstellar dust (Dwek 2006, and references therein). The dust formation efficiency depends on a multitude of factors that determine the abundance of refractory elements, and the evolution of the gas density, temperature, and ionization fraction in the ejecta. Calculating the yield of dust in supernova (SN) ejecta poses a particular theoretical challenge because of the presence of radioactive nuclei that generate a cascade of high-energy photons and non-thermal electrons that have an important effect on the chemical reaction and nucleation rates in the ejecta. Numerous models have been developed to calculate the production of dust in CCSNe (Clayton 1979; Todini & Ferrara 2001; Bianchi & Schneider 2007; Cherchneff 2013; Nozawa & Kozasa 2013; Sarangi & Cherchneff 2015; Sluder et al. 2018). A common result of all models is that about half of the final dust mass is formed within 2–3 yr after the explosion. The need for the early formation of dust is a natural consequence of the rapid decrease in the density and temperature of the ejecta, which leads to prohibitively long timescales for the nucleation and growth of grains at late times.

The case for the early and rapid dust formation is supported by the early "disappearance" of refractory elements, such as Si, Mg, and Fe, from the ejecta of SN 1987A (Danziger et al. 1991; Lucy et al. 1991; Dwek et al. 1992). Although these disappearances could have been the results of their recombination, their concurrence with the appearance of the infrared (IR) excess in the SN light curve strongly suggests dust formation as the cause.

Circumstantial evidence for the need of early dust formation arises from the high temperatures required to form silicates. They are an important dust component in SN ejecta. In the

interstellar medium silicates are identified by the 9.7 and 18 μm features that arise from the Si–O stretching and O–Si–O bending modes in the SiO_4 tetrahedral structure. The formation of this structure requires temperatures in excess of ~1000 K for a period of ~1–2 days (Hallenbeck et al. 1998). These conditions are only attainable in SN ejecta during the first few years after the explosion.

Nonetheless, many researchers believe that dust formation is a slow process, and that most of the dust is formed at low temperatures, around 10–20 yr after the explosion. This scenario is founded on the widely cited Figure 4 in Gall et al. (2014), which shows a trend, hereafter referred to as the Mdust–Age trend, of increasing dust mass with SN age. In this figure, dust masses increase from a value of about $10^{-5}\ M_\odot$ at about a few years after the explosion to about 0.5 $M_\odot$ after a few decades. The latter value corresponds to the inferred dust mass in ejecta of SN1987A (Matsuura et al. 2015) on day ~8500 after the explosion. However, the figure includes mass estimates from several SNe IIn whose emission is dominated by IR echoes from pre-existing dust or emission from dust that was formed by the interaction of the SN shock wave with the ambient circumstellar medium (Andrews et al. 2011; Sarangi et al. 2018, E. Dwek et al. 2019, in preparation). In spite of the diverse sources of IR emission, the Mdust–Age trend has been widely interpreted as evidence for the slow and gradual formation of dust in SN ejecta (Wesson et al. 2015; Bevan & Barlow 2016; Krafton & Clayton 2017; Bevan 2018; Gall & Hjorth 2018).

In particular, Wesson et al. (2015) used the IR observations of SN 1987A to argue that dust formation in its ejecta proceeded slowly. This interpretation seems to be supported by the slow evolution of the asymmetry in the profiles of emission lines from the ejecta (Bevan & Barlow 2016; Bevan 2018). This asymmetry, manifested in the absorption of the red wings in the lines' profile, is commonly attributed to intervening absorption by newly forming dust in the ejecta

---

(e.g., Lucy et al. 1989, 1991; Gall et al. 2014). Using the slow evolution of the line asymmetries in SN 1987A, Bevan & Barlow (2016) concluded that only about 20% of the dust mass has formed by day 4000.

In this Letter we show that the apparent Mdust–Age trend actually reflects the evolutionary trend of the ejecta's IR opacity. This point can be illustrated by a simple playback of the observed dynamics of SN 1987A (Dwek & Arendt 2015). Expanding at a spherically averaged velocity of ~ 900 km s^{-1} (Indebetouw et al. 2014), the 200 μm opacity generated by 0.5 $M_\odot$ of ejecta dust at the age of ≈ 20 yr is about 0.4. This transparency allowed for the determination of dust mass at that epoch. However, during the early epochs of mid-IR observations (Bouchet et al. 1991; Dwek et al. 1992; Wooden et al. 1993), the same amount of dust in the ejecta would have a 20 μm opacity of about 9100 and 5700 on days 615 and 775, respectively (Dwek & Arendt 2015). A dust mass of 0.5 $M_\odot$ could therefore have easily been "hidden" in the optically thick ejecta at those early epochs. These conditions apply not only to SN 1987A, but to CCSNe in general, necessitating the re-evaluation of the evolution of dust mass in SN ejecta.

This Letter is organized as follows. In Section 2 we develop a simple model for the evolution of the ejecta opacity, showing that it can offer a natural explanation for the observed Mdust–Age trend. In Section 3 we present corroborative arguments for the rapid formation of dust in the ejecta. A brief summary of the Letter is presented in Section 4.

2. The Evolution of Ejecta Opacity

The dust mass, $M_d^{\rm obs}$, is inferred from the observed specific IR flux, $F_\nu^{\rm obs}(\lambda)$, using the relation

$$M_d^{\rm obs} = \frac{F_\nu^{\rm obs}(\lambda)\, D^2}{B_\nu(\lambda,\, T_d)\kappa(\lambda)} \qquad (1)$$

where D is the distance to the source, $\kappa(\lambda)$ is the dust mass absorption coefficient, and $B_\nu(\lambda,\, T_d)$ is the Planck function at wavelength λ and dust temperature T_d. Equation (1) assumes that the source is optically thin and all of the dust is "visible" to the observer.

The radial opacity, $\tau(\lambda,\, t)$, of a spherically expanding dusty ejecta at wavelength λ and time t is given by

$$\tau(\lambda,\, t) = \rho_d(t)R(t)\kappa(\lambda) = \frac{3}{4}\left(\frac{M_d(t)}{\pi R(t)^2}\right)\kappa(\lambda)$$

$$= \frac{3}{4}\left(\frac{M_d(t)}{\pi v_{\rm ej}^2}\right)\kappa(\lambda)t^{-2} \qquad (2)$$

where $\rho_d(t)$ and $M_d(t)$ are, respectively, the mass density and total mass of dust in the ejecta at time t and $R(t)$ is the radius reached by a freely expanding ejecta at a velocity $v_{\rm ej}$ at t.

The escape probability of an IR photon from a sphere of optical depth τ is given by Cox & Mathews (1969) and Osterbrock & Ferland (2006)

$$P_{\rm esc}(\tau) = \frac{3}{4\tau}\left[1 - \frac{1}{2\tau^2} + \left(\frac{1}{\tau} + \frac{1}{2\tau^2}\right)e^{-2\tau}\right] \qquad (3)$$

where the λ dependence of τ has been suppressed for sake of clarity. At large optical depths $P_{\rm esc}(\tau) \approx 3/4\tau$. It approaches a value of $\sim \exp(-3\tau/4)$ for $\tau \ll 1$.

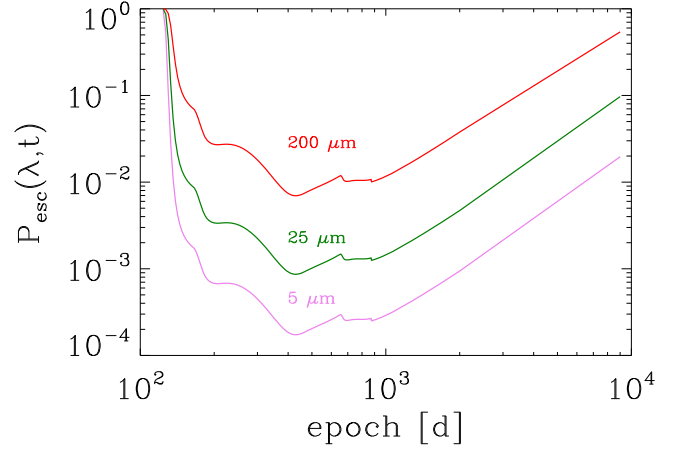**Figure 1.** Evolution of the escape probability, given by Equation (3), at different wavelengths.
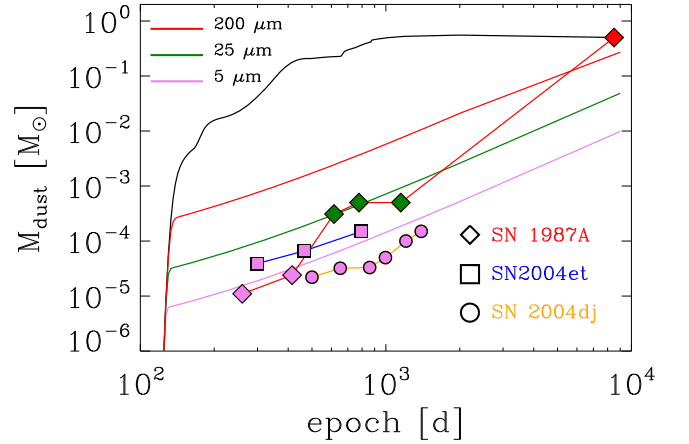

Figure 2. Growth of the dust mass in the ejecta of a 19 $M_\odot$ SN (black curve) is plotted against the epoch of observations, measured since the time of the explosion (Sarangi & Cherchneff 2015). The symbols represent the observationally inferred dust masses for various SNe that were observed for at least three epochs: SN 1987A (Dwek et al. 1992; Wooden et al. 1993; Matsuura et al. 2015; diamonds); SN 2004et (Kotak et al. 2009; squares); SN 2004dj (Kotak et al. 2005; Meikle et al. 2011; Szalai et al. 2011; circles). The different colored curves show the evolution of the inferred dust mass with ejecta opacity at three different wavelengths of observations. Observed dust masses were color coded according to the wavelength of observations.

Figure 1 shows the evolution of the escape probability at several wavelengths. In calculating τ, the mass absorption coefficient was represented by a λ^{-1} power law, normalized to a value of 10^3 cm g^{-1} at 5 μm. The expansion velocity of the ejecta was take to be of 10^3 km s^{-1}, approximately equal to the spherically averaged expansion velocity of the ejecta of SN 1987A (Indebetouw et al. 2014). The evolution of the ejecta dust mass was taken from Sarangi & Cherchneff (2015). It is shown in Figure 2 and described in more detail below. Figure 1 shows that the ejecta is transparent at the onset of dust formation, but becomes rapidly opaque after day ~ 150.

The observed flux, $F_\nu^{\rm obs}(\lambda)$, is given by $F_\nu^{\rm obs}(\lambda) = F_\nu^0(\lambda)P_{\rm esc}(\tau)$, where $F_\nu^0(\lambda)$ is the unobscured flux from the ejecta. The observed dust mass at time t observed at a given wavelength λ, $M_d^{\rm obs}(\lambda,\, t)$, derived from the optically thin

assumption, is related to the total dust mass by

$$M_d^{\rm obs}(\lambda, t) = \frac{F_\nu^0(\lambda) P_{\rm esc}(\tau) \, D^2}{B_\nu(\lambda, T_d) \kappa(\lambda)}$$
$$= M_d(t) \times P_{\rm esc}(\tau) \qquad (4)$$

Equation (4) illustrates the degeneracy between the dust mass in the ejecta and the optical depth. Different combinations of M_d and $P_{\rm esc}(\tau)$ can yield the same observed dust mass. Previous studies that concluded that the ejecta is optically thin (e.g., Wooden et al. 1993; Meikle et al. 2011) made this assumption implicitly in their calculations.

When the ejecta is optically thick, $P_{\rm esc}(\tau) = 3/4\tau$, and substituting the expression for τ from Equation (2), Equation (4) can be written as

$$M_d^{\rm obs}(\lambda, t) = \frac{3M_d}{4\tau} = \frac{\pi R(t)^2}{\kappa(\lambda)}$$
$$= \pi \rho_d(t) R(t)^2 h(t) = \left[\frac{\pi v_{\rm ej}^2}{\kappa(\lambda)}\right] t^2 \qquad (5)$$

where $h \equiv (\rho_d \, \kappa)^{-1}$ is the depth at which the ejecta's atmosphere reaches a value of $\tau = 1$. Equation (5) shows that at high optical depths the "visible" dust mass is independent of the actual dust mass, and that it increases as t^2.

Figure 2 (black curve), taken from Sarangi & Cherchneff (2015, their Figure 10), depicts the growth of the dust mass in the ejecta of a 19 $M_\odot$ progenitor star calculated with a detailed chemical reaction/dust formation network (Cherchneff & Dwek 2009; Cherchneff 2010; Sarangi & Cherchneff 2013). The calculated dust mass was normalized to reproduce the inferred dust mass of SN 1987A at late epochs. A similar evolutionary profile for the evolution of dust mass in SN 1987A was recently derived by Sluder et al. (2018, their Figure 15). Figure 2 represents the dust mass, given by $M_d(t) \times P_{\rm esc}(\tau)$. The escape probability is wavelength dependent, and the different colored lines depict the evolution of $M_d^{\rm obs}$ at different wavelengths. The figure shows that at each wavelength, $M_d^{\rm obs}(t)$ rapidly approaches the t^2 behavior given by Equation (5) for $\tau \gg 1$.

The colored symbols represent the inferred dust masses for several SNe. The IR spectrum of SN 1987A was observed around the peak wavelength of the emission, at about 5 μm on days 260 and 415, ~10 μm on days 615 and 775, ~25 μm on day 1140, and at ~200 μm on day 9000. The inferred dust masses are in very good agreement with those expected at the observed wavelengths. SN 2004et and SN 2004dj were observed with the IR Array Camera instrument on board the *Spitzer* spacecraft. The 3.6–8 μm emission is dominated by ejecta dust, whereas the emission at longer wavelength emission may be an IR echo from the SN ultraviolet (UV)-optical (UVO) light curve (Meikle et al. 2011). The figure shows that the inferred dust masses from these SNe agree well with the calculated visible dust mass at 5 μm, roughly the peak of the ejecta dust emission.

Overall, the figure shows a good agreement between the inferred dust mass and that predicted from Equation (5) at the observed wavelengths. In particular, the data follow the predicted t^2 behavior. Offsets of different SNe from the theoretical Mdust–age curve along the y-axis reflect the different expansion velocities and different dust compositions, leading to different values of κ.

In Gall et al. (2014), the evolution in the ejecta dust mass was approximated by a broken power law. However, emission prior to day ∼ 240, the date of the break in the power law, cannot be attributed to newly formed ejecta dust. Calculations (e.g., Sarangi & Cherchneff 2015; Sluder et al. 2018) and observations of SN 1987A (Wooden et al. 1993) show that dust formation commences only after day ∼250, when the ejecta has cooled sufficiently. Data prior to this epoch is affected by emission caused by an echo from pre-existing circumstellar dust (e.g., Bode & Evans 1980; Dwek 1983). Data beyond this epoch are not well sampled, except for SN 1987A which, as shown in Figure 2, clearly exhibits a t^2 behavior.

For clarity, all calculations presented above assumed a homogeneous ejecta expanding at a constant velocity. 3D hydrodynamic simulations of SN explosions show that instabilities generated by the expanding radioactive Ni–Co bubble will cause the ejecta to fragment into clumps (Wongwathanarat et al. 2015, and references therein). The early escape of gamma- and X-ray emission from SN 1987A provided observational evidence for large-scale instabilities and mixing in the ejecta (see the review by McCray & Fransson 2016). The IR emission from a clumpy ejecta was discussed in detail by Dwek & Arendt (2015). When the clump filling factor remains unchanged, a clumpy ejecta will exhibit the same trend of evolving opacity as a homogeneous one, as each expanding clump becomes optically thin. The t^2 behavior of the Mdust–Age trend exhibited in this Letter will thus remain unchanged for a clumpy ejecta.

So far we attributed the low inferred dust mass to the IR opacity of the ejecta. We illustrated this point in Dwek & Arendt (2015) by assuming that the silicate and carbon grains each have distinct single temperatures. Their emission peaks at around the wavelengths of observations, so that all dust is, in principle, equally observable. Alternatively, the low inferred dust mass could reflect the fact that most of the dust in the ejecta is cold, and therefore not observable with the mid-IR wavelengths used at the early epochs of observations. Such a possibility will give further support for the early and rapid formation of dust in the ejecta. However, modeling such a scenario will require detailed knowledge of the relative spatial distribution of the radioactivity and the dust, and is beyond the scope of this Letter.

3. The Growth of Dust Mass in SN Ejecta

IR observations of SN 1987A show the appearance of an IR emission component, in excess of the photospheric emission, within a year of the explosion (Wooden et al. 1993). The appearance of the IR excess coincided with the sudden drop in the Mg I 0.4571μm and [Si I] 1.65μm emission lines around day 530 (Danziger et al. 1991; Lucy et al. 1991), and a drop in the bolometric luminosity of the SN (Whitelock et al. 1989). These observations strongly suggest that the IR emission originated from silicate dust that formed rapidly and efficiently in the ejecta, and that caused the partial obscuration of the UVO output from the SN. The absence of the 9.7 and 18 μm silicate features in the spectra is the result of self absorption in the optically thick ejecta in the model of Dwek & Arendt (2015). Alternatively, Wesson et al. (2015) argued that the absence of the silicate features is caused by the dominance of the emission from featureless carbon dust, which will require carbon to be the dominant dust species formed in the

ejecta, contrary to theoretical model predictions (Sarangi & Cherchneff 2015; Sluder et al. 2018).

The early appearance of a broad emission feature in the 8–14 μm spectrum of SN 2004et on day 300 also provides evidence for the early formation of dust in SN ejecta (Kotak et al. 2009). The feature, and its related photometric 8 μm excess over that of a blackbody spectrum, persisted through day 690 and faded thereafter. The feature is attributed to silicate dust emission, and its decline could be the results of a drop in dust temperature. Observations of SN 1987A show that after day 600 the dust temperature has dropped below $\sim$400 K (Wooden et al. 1993), the temperature at which the emission peaks around 8 μm. The drop in dust temperature could result from the decline in the radioactive heating source or the growth of the dust grains. The decline of the feature could also have been caused by the growth of the silicate grains to a radius of a few microns, above which they become opaque to their own feature.

The early and rapid formation of dust in SN ejecta is also widely supported by theoretical models for the formation of dust in SN ejecta (e.g., Todini & Ferrara 2001; Cherchneff 2010; Nozawa et al. 2010; Sarangi & Cherchneff 2015). Most recent molecular nucleation models for the formation of dust in SN 1987A show that most of the dust formed before day 1000 after the explosion (Sluder et al. 2018, their Figure 10). Their computed dust formation rate agrees with the early dust formation model, and does not support the gradual formation scenario of Wesson et al. (2015) and Bevan & Barlow (2016).

The strongest argument for the slow formation of dust in the ejecta of SN 1987A is the evolution of the ejecta line asymmetries (Bevan & Barlow 2016). However, their model adopts a spherically symmetric expanding ejecta, whereas resolved 2012 observations of the SN with the Atacama Large Millimeter/submillimeter Array (ALMA) suggests a clumpy elongated structure (Indebetouw et al. 2014). Late time observations (day 10,000) of the Hα and the blended [Si I] +[Fe II] line emission from SN 1987A were used to construct a 3D model for the distribution of the emitting material (Larsson et al. 2016). The observations show that the blended 1.644 μm line is asymmetric with a prominent redshifted component, which is inconsistent with the Bevan & Barlow (2016) model predictions. The 3D distribution of the [Si I]+[Fe II] line reveals an elongated structure that is consistent with the ALMA observations but with a gap at the center, which is not detectable in the ALMA image due to projection effects. These results suggest that the models of Bevan & Barlow (2016) and Bevan (2018) are at least incomplete, and not robust enough to corroborate a scenario for the slow and gradual formation of dust in the ejecta. A more complex model consisting of a clumpy asymmetrically expanding ejecta is required to obtain a consistent picture for the evolution of the line profiles from the ejecta.

The detection of a ^{49}Ti excess in presolar SiC grains of SN origin, commonly referred to as X-grains, was interpreted as evidence for the late formation of silicate carbide in SNe II (Liu et al. 2018). Detailed calculations show that ^{49}Ti must have been incorporated in the grains not sooner than 2 yr after the explosion (Liu et al. 2018), which is in agreement with theoretical calculations showing that SiC grains are late to form in the ejecta (Sarangi & Cherchneff 2015). Figure 2 shows that at that epoch more than 50% of the dust has already formed in

the ejecta. The mass of SiC dust grains is about $10^{-4}\,M_\odot$, and the mass of all Ti isotopes is about $10^{-4}\,M_\odot$ (Nomoto et al. 2013). The X-grains make therefore a negligible contribution to the total dust mass in the ejecta. The ^{49}Ti anomaly is therefore an excellent chronometer for the formation time of the X-grains, but has no bearing on the epoch of the bulk of the dust formation in the SN ejecta.

4. Summary

In this Letter we have offered a natural explanation for the Mdust–Age trend for CCSNe. The observable dust mass constitutes only a small fraction of the total mass, namely that present in the "photosphere," the volume where $\tau_{\rm IR} < 1$, of the IR-thick ejecta. As the ejecta expands its optical depth decreases as $R(t)^{-2} \sim t^{-2}$, which is consistent with the observed Mdust–Age trend. We therefore propose an alternate scenario in which most of the dust forms within two year after the explosion. The IR emission from the dust is initially self absorbed, revealing most of the dust mass only decades after the expansion (Dwek & Arendt 2015). The rapid formation of dust in the ejecta is consistent with the observed depletion of refractory elements concomitant with the early dust emission and the drop in the bolometric luminosity from some SNe. It is also consistent with theoretical models, in which most of the dust forms during the early phases of the expansion when ejecta densities and temperatures are high enough to form the necessary chemical bonds and support the reaction rates needed to grow the nucleation seeds.

Our scenario also offers a simple solution to the conflict between theoretical calculations that show the dominance of silicate dust over carbon (e.g., Sluder et al. 2018), and the models of Wesson et al. (2015) and Bevan & Barlow (2016), in which carbon is the dominant dust species. In our scenario, the lack of the 9.7 and 18 μm silicate emission features in the spectra of SN 1987A is not evidence for the absence of silicate dust, but merely a manifestation of the optical depth of the ejecta (Dwek & Arendt 2015).

The results of this Letter have important implications for determining the physical conditions in SN ejecta. Modeling the UVO–near-IR emission from SN 1987A requires calculations of the energy cascade that degrades the γ-rays and positrons into UV and optical and IR line emission. These detailed calculations were done with the assumption that the dust opacity is low (Jerkstrand et al. 2011). However, because of the significantly large UVO optical depth, the competition between the dust and atomic species for the absorption of these photons must now be taken into account.

Dedicated ground-based or satellite (e.g., the *James Webb Space Telescope*) observations of young SNe in local galaxies at $z \lesssim 0.2$, over a period of several years will provide the much needed observations to confirm the t^2 trend in Mdust–Age relation.

ORCID iDs

Eli Dwek ⬤ https://orcid.org/0000-0001-8033-1181
Arkaprabha Sarangi ⬤ https://orcid.org/0000-0002-9820-679X
Richard G. Arendt ⬤ https://orcid.org/0000-0001-8403-8548

References

Andrews, J. E., Clayton, G. C., Wesson, R., et al. 2011, AJ, 142, 45
Bevan, A. 2018, MNRAS, 480, 4659
Bevan, A., & Barlow, M. J. 2016, MNRAS, 456, 1269
Bianchi, S., & Schneider, R. 2007, MNRAS, 378, 973
Bode, M. F., & Evans, A. 1980, MNRAS, 193, 21P
Bouchet, P., Phillips, M. M., Suntzeff, N. B., et al. 1991, A&A, 245, 490
Cherchneff, I. 2010, in ASP Conf. Ser. 425, Hot and Cool: Bridging Gaps in
    Massive Star Evolution, ed. C. Leitherer et al. (San Francisco, CA:
    ASP), 237
Cherchneff, I. 2013, PoS, LCDU2013, 18
Cherchneff, I., & Dwek, E. 2009, ApJ, 703, 642
Clayton, D. D. 1979, Ap&SS, 65, 179
Cox, D. P., & Mathews, W. G. 1969, ApJ, 155, 859
Danziger, I. J., Lucy, L. B., Bouchet, P., & Gouiffes, C. 1991, in Supernovae,
    The Tenth Santa Cruz Workshop in Astronomy and Astrophysics, ed.
    S. E. Woosley (New York: Springer), 69
Dwek, E. 1983, ApJ, 274, 175
Dwek, E. 2006, Sci, 313, 178
Dwek, E., & Arendt, R. G. 2015, ApJ, 810, 75
Dwek, E., Moseley, S. H., Glaccum, W., et al. 1992, ApJL, 389, L21
Gall, C., & Hjorth, J. 2018, ApJ, 868, 62
Gall, C., Hjorth, J., Watson, D., et al. 2014, Natur, 511, 326
Hallenbeck, S. L., Nuth, J. A., & Daukantas, P. L. 1998, Icar, 131, 198
Indebetouw, R., Matsuura, M., Dwek, E., et al. 2014, ApJL, 782, L2
Jerkstrand, A., Fransson, C., & Kozma, C. 2011, A&A, 530, A45
Kotak, R., Meikle, P., van Dyk, S. D., Höflich, P. A., & Mattila, S. 2005, ApJL,
    628, L123
Kotak, R., Meikle, W. P. S., Farrah, D., et al. 2009, ApJ, 704, 306
Krafton, K., & Clayton, G. C. 2017, MmSAI, 88, 416
Larsson, J., Fransson, C., Spyromilio, J., et al. 2016, ApJ, 833, 147
Liu, N., Nittler, L. R., Alexander, C. M. O., & Wang, J. 2018, SciA, 4,
    eaao1054
Lucy, L. B., Danziger, I. J., Gouiffes, C., & Bouchet, P. 1989, in IAU Coll.
    120, Structure and Dynamics of the Interstellar Medium, Vol. 350, ed.
    G. Tenorio-Tagle, M. Moles, & J. Melnick (Berlin: Springer), 164
Lucy, L. B., Danziger, I. J., Gouiffes, C., & Bouchet, P. 1991, in Supernovae,
    The Tenth Santa Cruz Workshop in Astronomy and Astrophysics, ed.
    S. E. Woosley (New York: Springer), 82
Matsuura, M., Dwek, E., Barlow, M. J., et al. 2015, ApJ, 800, 50
McCray, R., & Fransson, C. 2016, ARA&A, 54, 19
Meikle, W. P. S., Kotak, R., Farrah, D., et al. 2011, ApJ, 732, 109
Nomoto, K., Kobayashi, C., & Tominaga, N. 2013, ARA&A, 51, 457
Nozawa, T., & Kozasa, T. 2013, ApJ, 776, 24
Nozawa, T., Kozasa, T., Tominaga, N., et al. 2010, ApJ, 713, 356
Osterbrock, D. E., & Ferland, G. J. 2006, Astrophysics of Gaseous Nebulae
    and Active Galactic Nuclei (Mill Valley, CA: Univ. Science Books)
Sarangi, A., & Cherchneff, I. 2013, ApJ, 776, 107
Sarangi, A., & Cherchneff, I. 2015, A&A, 575, A95
Sarangi, A., Dwek, E., & Arendt, R. G. 2018, ApJ, 859, 66
Sluder, A., Milosavljević, M., & Montgomery, M. H. 2018, MNRAS,
    480, 5580
Szalai, T., Vinkó, J., Balog, Z., et al. 2011, A&A, 527, A61
Todini, P., & Ferrara, A. 2001, MNRAS, 325, 726
Wesson, R., Barlow, M. J., Matsuura, M., & Ercolano, B. 2015, MNRAS,
    446, 2089
Whitelock, P. A., Catchpole, R. M., Menzies, J. W., et al. 1989, MNRAS,
    240, 7P
Wongwathanarat, A., Müller, E., & Janka, H.-T. 2015, A&A, 577, A48
Wooden, D. H., Rank, D. M., Bregman, J. D., et al. 1993, ApJS, 88, 477